

Hyperspectral image segmentation, deblurring, and spectral analysis for material identification

Fang Li^a, Michael K. Ng^b, Robert Plemmons^c, Sudhakar Prasad^d, Qiang Zhang^e

^a Dept. Mathematics, East China Normal University, Shanghai 200062, PR China;

^b Dept. Mathematics, Hong Kong Baptist University, Kowloon Tong, Hong Kong;

^c Depts. Math. & Computer Science, Wake Forest University, Winston-Salem, NC 27106;

^d Dept. Physics and Astronomy, University of New Mexico, Albuquerque, NM 87131;

^e Dept. Biostatistical Sciences, Wake Forest University, Winston-Salem, NC 27109

ABSTRACT

An important aspect of spectral image analysis is identification of materials present in the object or scene being imaged. Enabling technologies include image enhancement, segmentation and spectral trace recovery. Since multi-spectral or hyperspectral imagery is generally low resolution, it is possible for pixels in the image to contain several materials. Also, noise and blur can present significant data analysis problems. In this paper, we first describe a variational fuzzy segmentation model coupled with a denoising/deblurring model for material identification. A statistical moving average method for segmentation is also described. These new approaches are then tested and compared on hyperspectral images associated with space object material identification.

Keywords: Hyperspectral Data, Segmentation, Deblurring, Denoising, Dimensionality Reduction, Classification, Spectral Mixture Analysis

1. INTRODUCTION

Three major objectives in processing hyperspectral image data of an object (target) are data compressive representation, spectral signature identification of constituent materials, and determination of their corresponding fractional abundances. Hyperspectral remote sensing technology allows one to capture images using a range of spectra from ultraviolet to visible to infrared. Multiple images of a scene or object are created using light from different parts of the spectrum. These hyperspectral images can be used, for example, to detect and identify objects at a distance, to identify surface minerals, objects and buildings from space, and to enable Space Object Identification (SOI) from the ground. In this particular study within the domain of SOI, we concentrate on hyperspectral image deblurring, segmentation, and object material identification.

Zhang, Wang, Plemmons and Pauca¹ have proposed a novel approach to processing hyperspectral data (tensors) using Nonnegative Tensor Factorization (NTF) for 3-D arrays, which reduces a large tensor into three nonnegative factor matrices. This approach preserves physical characteristics of the data such as nonnegativity and is a natural extension of nonnegative least squares approximate nonnegative matrix factorization.² However, the use of NTF was only partially successful. Hyperspectral data is typically noisy and suffers for both spatial and spectral blurring.³⁻⁷ Also, analyzing tensors is challenging. Algorithms fitting tensor models depend heavily upon the initial set-up, i.e., number of components, and the initialization of the component matrices. (See the NSF Workshop report by Van Loan⁸ for a discussion of tensor computations and research needed for these problems.)

E-mail address of corresponding author Robert Plemmons: plemmons@wfu.edu. Research by Li was supported in part by the National Science Foundation of Shanghai (10ZR1410200). Research by Ng was supported in part by RGC 201508 and HKBU FRGs. Research by Plemmons, Prasad, and Zhang was supported in part by the U.S. Air Force Office of Scientific Research (AFOSR), with award number FA9550-08-1-0151. The scientific responsibility is assumed by the authors.

In this paper we propose alternatives to the use of NTF for hyperspectral data analysis with space object material identification applications. We apply segmentation and deblurring models to the problem of hyperspectral material (sometimes called endmember) identification. In Section 2 a variational-based coupled segmentation and deblurring model is proposed, and the numerical implementation of the proposed method is described for hyperspectral data. Next, we discuss a new statistical moving average method for hyperspectral segmentation in Section 3. We then describe the hyperspectral data used for our numerical tests and relationships to the space object identification problem in Section 4, and numerical experiments and comparisons are provided. Some comments and open problems are given in Section 5.

2. JOINT SEGMENTATION AND RESTORATION

The enormity of direct data storage and processing tasks for hyperspectral data is often too daunting to permit a reasonable direct computational approach. This is particularly true in the context of computing information measures for highly-multi-parametric statistical distributions, and where the data are blurred and noisy across the spectral bands. A different and more practical approach in this case is one that stresses physics in the specific sense that the underlying physical model is often based on a rather much smaller set of parameters. A powerful strategy in handling what are naively large data sets is thus to devote considerable attention to the underlying physical model and to identify the small set of parameters that can explain the underlying structure of the otherwise intractable data volume. The viability of this approach is guaranteed very generally, since physical problems of any interest very often admit a complete description in terms of a relatively small set of parameters.

A useful approach to extracting and processing such underlying structure is to employ image segmentation and object identification techniques to compressively represent the original hyperspectral cubes by a set of spatially orthogonal bases and a set of spectral traces, i.e.

$$\mathcal{T}(x, y, \lambda) \approx \sum_i \mu_i(x, y) f_i(\lambda), \quad (x, y) \in \Omega, \quad (1)$$

where Ω is the domain of the observed hyperspectral cubes, $\mu_i(x, y)$ is a binary support function for the i^{th} object and $f_i(\lambda)$ is the spectral trace of the i^{th} object. This is the simpler case of assuming no overlapping between objects in the spatial dimensions, i.e., the $\{\mu_i\}$ are orthogonal, but it can be extended to the mixing case by changing the range of μ_i from binary to the interval of $[0, 1]$.

We anticipate a decomposition of the data into a sum of elementary images, each corresponding, e.g., to a specific material constituent of the surface of an object which can be expected to be spatially sparse in our applications. For example, in hyperspectral imaging of satellites from the ground, the μ_i could correspond to the solar panels which are localized to certain surface regions and are thus sparse over the full 2D array and the vector $f_i(\lambda)$ could correspond to a solar panel material spectral signature.¹ Variational PDE methods, e.g. the Chan-Vese model⁹ and its extensions,¹⁰ can be employed to segment out certain regions of a single image to identify μ_i .

From a practical standpoint hyperspectral data is generally noisy and blurred, especially in ground-based imaging through the atmosphere.^{3,4} This situation can complicate any attempt to segment and analyze the data, as was observed Zhang, et al.¹ We first describe a denoising/deblurring model that will be used to preprocess the hyperspectral data, along with segmentation.

2.1 Fast Denoising/Deblurring Model using Variational Methods

Image restoration and reconstruction play an important part in numerous areas of applied sciences such as medical and astronomical imaging, image and video coding, etc. In our particular application we are concerned with the degradation effects of imaging through atmospheric turbulence.¹¹

Suppose the observed gray scale image $I_0 : \Omega \rightarrow \mathcal{R}$ is blurred with a known point spread function (psf) h and contaminated by some noise η , that is

$$I_0(x, y) = (h * I)(x, y) + \eta(x, y). \quad (2)$$

We assume h satisfies $h \geq 0$ and $\int_{\Omega} h(x, y) dx dy = 1$. In order to recover the clean image I from I_0 , a total variation regularization with ℓ_2 fit-to-data term deblurring model minimizes the following energy functional

$$E(I) = \int_{\Omega} |\nabla I| dx dy + \gamma \int_{\Omega} (h * I - I_0)^2 dx dy.$$

The first term in the right hand side is the total variation of I . Huang, et al.¹² proposed to introduce an auxiliary variable J , and to approximate the energy $E(I)$ by

$$E(I, J) = \int_{\Omega} |\nabla J| dx dy + \frac{1}{2\theta} \int_{\Omega} (I - J)^2 dx dy + \gamma \int_{\Omega} (h * I - I_0)^2 dx dy.$$

Then they solve the minimizer by an alternative minimization method: Fixing I , J can be solved by Chambolle's¹³ fast dual projection method; Fixing J , I can be solved in various ways, for example using the FFT when h is spatially invariant. The overall algorithm is faster than gradient descent methods.¹² Here, θ and γ are fixed parameters defined by the user. The parameters can be determined by using the strategy studied by Liao, et al.¹⁴ We adopt the above deblurring/denoising model here.

2.2 A Fuzzy Piecewise Constant Segmentation Model

A crucial problem in image analysis is to partition a given image into disjoint regions, such that the regions correspond to objects in the image. There are a wide variety of approaches to the segmentation problem. Based on the Mumford-Shah¹⁵ functional for segmentation, Chan and Vese⁹ proposed a level set model for active contours to detect objects whose boundaries are not necessarily defined by a gradient.

As in the Chan-Vese model,⁹ we assume the image can be approximated by a piecewise constant function $\sum_{i=1}^N c_i \chi_i$ where χ_i is the characteristic function of set Ω_i and c_i are constants, i.e.,

$$I(x, y) \approx c_i, \quad (x, y) \in \Omega_i,$$

where $\{\Omega_i\}_{i=1}^N$ is a partition of the image domain Ω . Then the piecewise constant segmentation problem becomes to recover the clean image I , $c = (c_1, \dots, c_n)$ and the partition from the observed data I_0 . According to (1), we determine Ω_i and c_i to match the λ th frequency image of the hyperspectral tensors as follows:

$$c_i = \begin{cases} f_i(\lambda), & (x, y) \in \Omega_i \text{ with } \mu_i(x, y) = 1 \\ 0, & \text{otherwise.} \end{cases}$$

For convenience, we label the background to be one region or one material. In the following discussion, we consider segmentation and deblurring model for the λ th frequency image of the hyperspectral cubes. The extension of the model to the whole hyperspectral tensor with all frequencies will be considered later.

Let $\partial\Omega_i$ be the boundary of region Ω_i . Let $\Gamma = \bigcup_{i=1}^N \partial\Omega_i$ be the segmentation boundaries of the entire image. The segmentation is usually given by minimizing the piecewise constant Mumford-Shah energy functional

$$E(c, \Gamma) = |\Gamma| + \sum_{i=1}^N \tau \int_{\Omega_i} (I - c_i)^2 dx dy. \quad (3)$$

In terms of characteristic functions $\chi = (\chi_1, \dots, \chi_N)$, where χ_i denotes the characteristic function of region Ω_i , energy (3) can be rewritten as

$$E(c, \chi) = \sum_{i=1}^N \int_{\Omega} |\nabla \chi_i| dx dy + \sum_{i=1}^N \tau \int_{\Omega} (I - c_i)^2 \chi_i dx dy. \quad (4)$$

Here $\int_{\Omega} |\nabla \chi_i| dx dy$ equals the perimeter of $\partial\Omega_i$. There is a scaling of factor 2 since we add each boundary twice. For simplicity, we neglect it.

The binary valued function χ_i gives a hard segmentation of Ω . In the following, we use a fuzzy membership function $u_i(x, y)$ to substitute for the hard membership function χ_i in (4). As a fuzzy membership function, u_i must satisfy the conditions:

$$(i) \quad 0 \leq u_i \leq 1, \quad \text{and} \quad (ii) \quad \sum_{i=1}^N u_i = 1. \quad (5)$$

Then we get the constrained fuzzy piecewise constant segmentation model of minimizing energy functional

$$E(U, c) = \sum_{i=1}^N \int_{\Omega} |\nabla u_i| dx dy + \sum_{i=1}^N \tau \int_{\Omega} (I - c_i)^2 u_i^p dx dy \quad (6)$$

where p is a parameter to determine the fuzziness of segmentation and $U = (u_1, \dots, u_N)$.

For image without noise and/or blur, the fuzzy piecewise constant segmentation model generally works quite well,¹⁷ and we adopt that model here.

2.3 Combined Model and Numerical Method for Solution

We now combine the denoising/deblurring model and the fuzzy piecewise constant segmentation model, and set $p = 2$. This leads to a coupled model for deblurring and segmentation which is to minimize

$$\begin{aligned} E(U, c, I) = & \int_{\Omega} |\nabla I| dx dy + \sum_{i=1}^N \int_{\Omega} |\nabla u_i| dx dy + \frac{\gamma}{2} \int_{\Omega} (h * I - I_0)^2 dx dy + \\ & \sum_{i=1}^N \frac{\tau}{2} \int_{\Omega} (I - c_i)^2 u_i^2 dx dy \end{aligned} \quad (7)$$

subject to constraints (i) and (ii) in (5).

Next, we provide a numerical method for minimizing (7). For efficiency, we choose to follow Huang, et al.¹² and use Chambolle's dual projection algorithm.¹³ Adding auxiliary variables $V = (v_1, \dots, v_N)$ and J , we approximate E by

$$\begin{aligned} E_r(I, J, U, V, c) = & \int_{\Omega} |\nabla J| dx dy + \sum_{i=1}^N \int_{\Omega} |\nabla v_i| dx dy + \frac{1}{2\eta} \int_{\Omega} (I - J)^2 dx dy \\ & + \frac{1}{2\theta} \sum_{i=1}^N \int_{\Omega} (v_i - u_i)^2 dx dy + \frac{\gamma}{2} \int_{\Omega} (h * I - I_0)^2 dx dy + \sum_{i=1}^N \frac{\tau}{2} \int_{\Omega} (I - c_i)^2 u_i^2 dx dy \end{aligned} \quad (8)$$

where θ and η are chosen small enough so that I and J , u_i and v_i are almost identical. Since (8) is componentwise convex in each variable I, J, U, V, c , we can minimize it by an alternating iteration method as follows.

1. Solve for the vector of constants c .
2. Solve for the auxiliary variable V .
3. Solve for the membership function U .
4. Solve for the auxiliary variable J .
5. Solve for the image I .

Details for these steps can be found in Li, Ng, and Plemmons.¹⁷

2.4 Hyperspectral DataCubes

Here we present the extension of our algorithm to three-dimensional tensors, specifically hyperspectral datacubes. Let $I(x, y, \lambda) : \Omega \times \mathcal{W} \rightarrow \mathcal{R}$ denote the tensor image where x and y denote spatial variables and λ is the spectral variable. In discrete form, we can view I as a vector-valued image as follows: $I = (I_1, \dots, I_m) : \Omega \rightarrow \mathcal{R}^m$. Here m is the number of spectral frequencies (wavelengths in spectral terminology) to be considered. The piecewise constant image model changes to

$$I_j(x, y) \approx c_{ij}, \quad j = 1 : m, \quad (x, y) \in \Omega_i$$

where $\{\Omega_i\}_{i=1}^N$ is a partition of the image domain Ω , and $c_i = (c_{i1}, \dots, c_{im})$ is a spectral vector of the i th object (or the spectrum of the i th object). Then, we can formulate a matrix $C = [c_{ij}]$ which denotes the spectral traces of all the segmented objects in the hyperspectral data cube. Note that these spectral traces, sometimes called endmembers, are determined here without matching with a spectral library as is often used.⁷

Similarly, consider the matrix $U = (u_1, \dots, u_N)$. The rows $u_i(x, y)$ of U are the fuzzy membership functions which are used to substitute for the hard membership functions χ_i in (4), and must satisfy (5).

Denote the observed hyperspectral tensor by I_0 . We combine the denoising/deblurring model and the fuzzy piecewise constant segmentation model together with $p = 2$, and consider a coupled model for denoising/deblurring and segmentation, which is to minimize

$$\begin{aligned} E(U, C, I) = & \sum_{j=1}^m \int_{\Omega} |\nabla I_j| dx dy + \sum_{i=1}^N \int_{\Omega} |\nabla u_i| dx dy + \frac{\gamma}{2} \int_{\Omega} (h * I - I_0)^2 dx dy + \\ & \sum_{i=1}^N \frac{\tau}{2} \int_{\Omega} d_i u_i^2 dx dy, \end{aligned} \quad (9)$$

subject to constraints (i) and (ii) in (5). Here $d_i = \frac{1}{m} \sum_{j=1}^m (I_j - c_{ij})^2$ refers to the average difference in the j th spectral band between the denoised/deblurred tensor image and the i th spectral object. The algorithm in the previous subsection can now be employed to the hyperspectral tensor case. For example, it is easy to obtain the new formulas for the components of the matrix C , i.e.,

$$c_{ij} = \frac{\int_{\Omega} I_j u_i^2 dx dy}{\int_{\Omega} u_i^2 dx dy}.$$

Then, the formulas for I_i, J_i are similar to I, J in the grayscale image case. The unknowns can be updated similarly according to the procedures discussed earlier.

Here we would like to remark that similar to a tensor decomposition of I , we can also interpret our decomposition of I by using the compressive representation matrices U and C as follows:

$$I_j(x, y) = \sum_{i=1}^N u_i(x, y) c_{ij}, \quad \forall (x, y) \text{ and } 1 \leq j \leq m.$$

3. A STATISTICAL MOVING AVERAGE METHOD

A particularly simple segmentation approach makes use of the spatial variation of spectral correlation in a typical hyperspectral dataset. Specifically, since according to the physical model (1) all spatial pixels of a given material in an image have the same normalized spectral trace, a coarse-grained spectral correlation function computed over a small moving 2D spatial cell of fixed shape and size will show sharp variations as the averaging cell crosses a boundary between two materials. The average normalized correlation function we use is defined as

$$\gamma(x, y) = \frac{1}{|\mathcal{C}|} \sum_{(x', y') \in \mathcal{C}} \frac{\sum_{\lambda} \mathcal{T}(x, y, \lambda) \mathcal{T}(x + x', y + y', \lambda)}{\sqrt{\sum_{\lambda} \mathcal{T}^2(x, y, \lambda)} \sqrt{\sum_{\lambda} \mathcal{T}^2(x + x', y + y', \lambda)}}, \quad (10)$$

where \mathcal{C} denotes the averaging cell and $|\mathcal{C}|$ the number of pixels it contains.

The use of the spectral correlation (10) reveals all material boundaries across the spatial image. To determine the boundaries of a specific material, say the i th material, we compute instead the average normalized cross-correlation function using the spectral trace $f_i(\lambda)$ of that material,

$$\gamma_i(x, y) = \frac{1}{|\mathcal{C}|} \sum_{(x', y') \in \mathcal{C}} \frac{\sum_{\lambda} f_i(\lambda) \mathcal{T}(x + x', y + y', \lambda)}{\sqrt{\sum_{\lambda} f_i^2(\lambda)} \sqrt{\sum_{\lambda} \mathcal{T}^2(x + x', y + y', \lambda)}}. \quad (11)$$

Note that since the spectral traces of dissimilar materials are in general poorly correlated, this cross-correlation will have the most significant value only over the material that corresponds to the chosen spectral trace. Repeating this procedure for the different spectral traces in the database, along with a simple thresholding to eliminate poorly correlated domains, then segments the image into its individual material components.

At a given spatial pixel, it is the variation of flux from one spectral channel to the next that contains a stronger material signature than the channel fluxes themselves. We therefore first pre-process the hyperspectral data by computing their spectral gradients in the various spectral channels before evaluating the correlation functions (10) and (11) for such spectral gradients.

Apart from its simplicity, the approach is largely forgiving of any flux variations from pixel to pixel of a specific material. In other words, in Eq. (1) the spatial factor $\mu_i(x, y)$ does not necessarily have to be a binary-valued function; the factorization of the summand into its spatial and spectral parts is all that is needed for the method to work.

The approach is also robust against noise and blur. Any zero-mean noise that is uncorrelated from pixel to pixel and one spectral channel to the next is essentially averaged to zero because of the joint spectral and spatial averaging contained in the expressions (10) and (11). Indeed, we can exploit this noise averaging to denoise an image before it is deblurred. The robustness against blur may be traced to the fact that for each material the method uses information in multiple spatial pixels and spectral channels, thus greatly constraining the segmentation problem. We illustrate both segmentation and denoising of images by applying our moving-average method to simulated hyperspectral datacubes in Section 4.3. A more detailed study of this approach will appear in Ref.¹⁶

4. NUMERICAL TESTS AND COMPARISONS

4.1 Simulated Hubble Space Telescope

We use an initial dataset of simulated spectral data using a 3-D model of the Hubble Space Telescope and a library of 262 material spectral signatures. These are lab-measured the absolute reflectance by comparing the measured reflectance of each material to a known reflectance of a white reference. The 3-D model was discretized into a 128×128 array of pixels for which a specific mixture of 8 materials was assigned based on orientation of the Hubble telescope. Figure 1 shows the spectral signatures of these materials. The signatures cover a band of spectrum from $.4\mu m$ to $2.5\mu m$ for 100 evenly distributed sampling points, leading to a data cube of size $128 \times 128 \times 100$.

Three other datasets were then constructed from the original by considering: i) spatial blur (Gaussian point spread function with standard deviation of 2 pixels), ii) noise (independent Gaussian, and signal-dependent Poisson noise associated with the light detection process), and iii) a mixture of blur and noise.

As an illustration of original material signatures assigned to each image pixel, we render an image of Hubble Space Telescope, Figure 2, using the color map defined in Table 1.

4.2 Coupled Segmentation and Deblurring/Denoising Results

First, we consider the denoising/deblurring performance. In the first row of Figure 3, the first band of the tensor image is shown. The second row shows the deblurred image using the fast denoising/deblurring model and the coupled model. It is clear that our coupled model has a similar performance as the denoising/deblurring model in the aspect of deblurring.

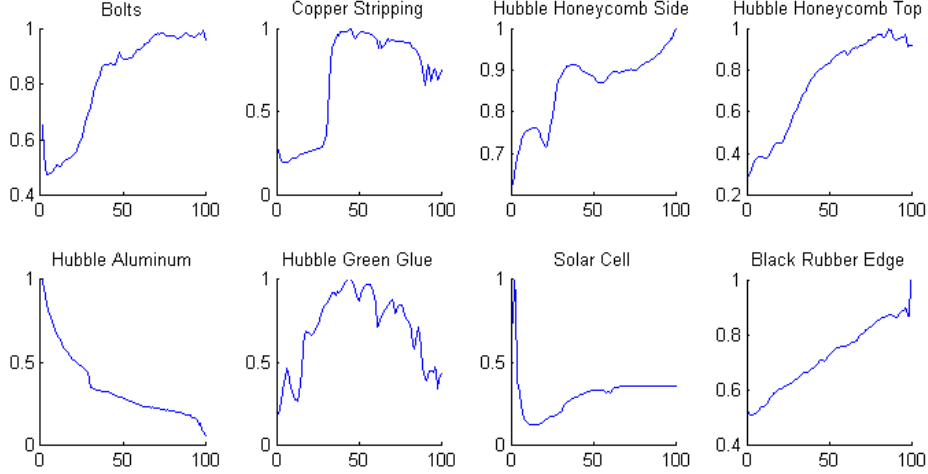


Figure 1. Spectral signatures of eight materials assigned to a Hubble Space Telescope model.

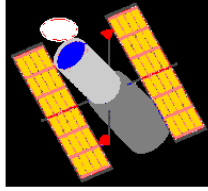


Figure 2. Materials assigned to pixels in Hubble Satellite Telescope image.

We have fully tested the coupled segmentation and deblurring/denoising algorithm on the four hyperspectral tensor images: the original clear image; the noisy image; the blurred image; the blurred and noisy image. The complete results are reported in Ref.¹⁷ Here, for brevity, we report mainly on the results for the original clear image and the blurred and noisy image, for comparison purposes.

In Figures 4 through 7, we test the clean and the blurred and noisy tensor images. We set $N = 9$, and give the segmentation results and the nine membership functions (including the background) in Figures 4 and 6. For instance, in Figures 4(a) and 6(a), the segmentation results refer to different regions based on the matrix U . In images (b) through (j), we show the values of the membership functions u_i . When the pixel intensity is white in the figures, this indicates that this pixel belong to a particular region in an image. Similarly, when the pixel intensity is black in the figures, this indicates that this pixel does not belong to the region formed. There may be some pixel intensities gray, which indicates that the pixel may or may not belong to the segmented region. As is usual, we choose the maximal value among all the membership functions to decide to which region this pixel belongs.

We show the original spectral signatures and the estimated spectral signatures for the membership functions in Figures 5 and 7. For these figures, the values of c_{ij} are shown with respect to region i of an image. Note that the estimated spectral signatures for Bolts and Black Rubber Edge are not matched well with the original signatures. The reason is that they are the smaller and thinner parts, and get mixed with surrounding materials which make them difficult to extract. However, the proposed method estimates the other materials very well. In the blurred and noisy tensor image, there are three materials (Bolts, Honeycomb Side and Black Rubber Edge) that are not matched very well, but the estimated spectral signatures of the other materials are quite good.

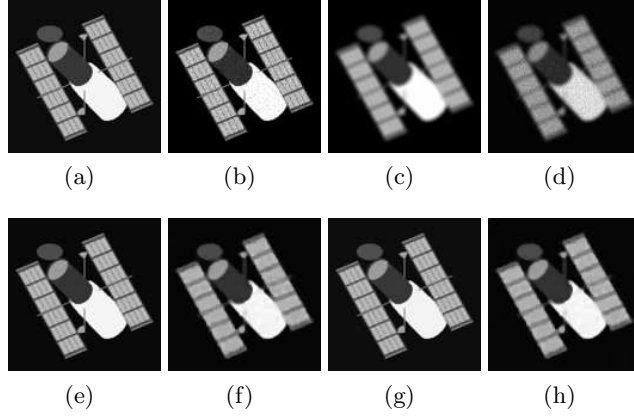


Figure 3. Band 1 of the hyperspectral tensor image. (a) the original clean image; (b) image with noise; (c) image with blur; (d) image with blur and noise; (e) deblurred image for (c) with our fast denoising/deblurring algorithm; (f) deblurred image for (d) with our fast denoising/deblurring algorithm; (g) deblurred image with coupled segmentation and deblurring algorithm for (c); (h) deblurred image with our denoising/deblurring algorithm for (d).

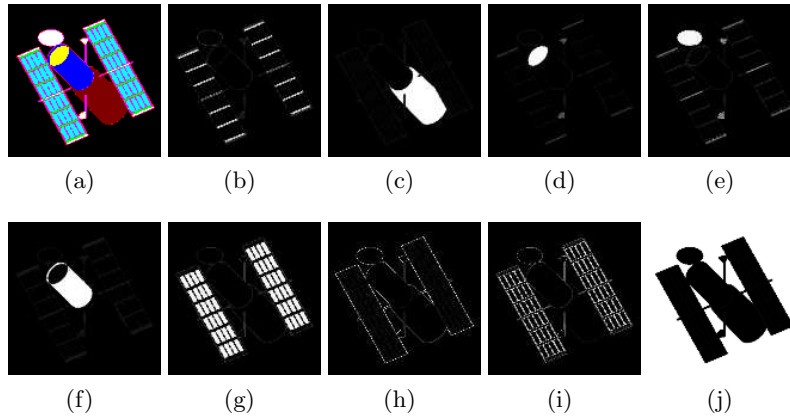


Figure 4. Segmentation of the clean tensor image; (a) the segmentation result; (b)-(j) the membership functions u_1 to u_9 .

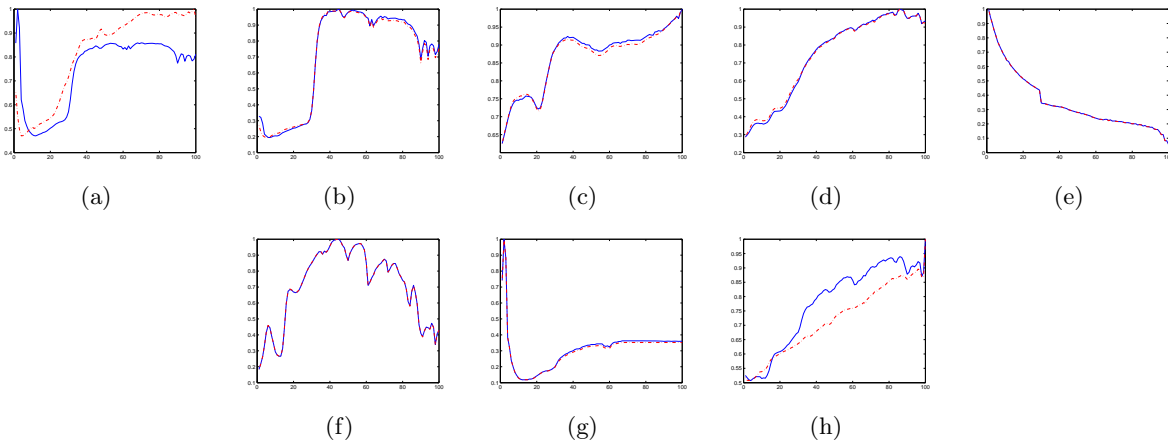


Figure 5. (The clean tensor image) The original material spectral signatures: red - and the estimated spectral signatures: blue and - : (a) Bolts; (b) Copper Stripping; (c) Hubble Honeycomb Side; (d) Hubble Honeycomb Top; (e) Hubble Aluminum; (f) Hubble Green Glue; (g) Solar Cell and (h) Black Rubber Edge.

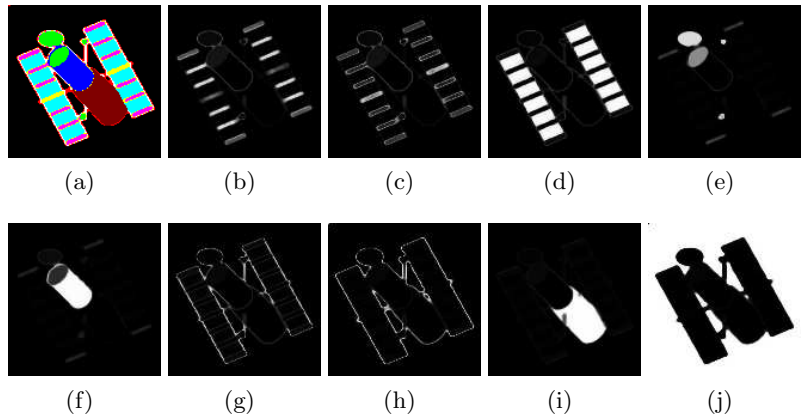


Figure 6. Segmentation of the blurred and noisy tensor image with the coupled segmentation and denoising/deblurring algorithm; (a) the segmentation result; (b)-(j) the membership functions u_1 to u_9 .

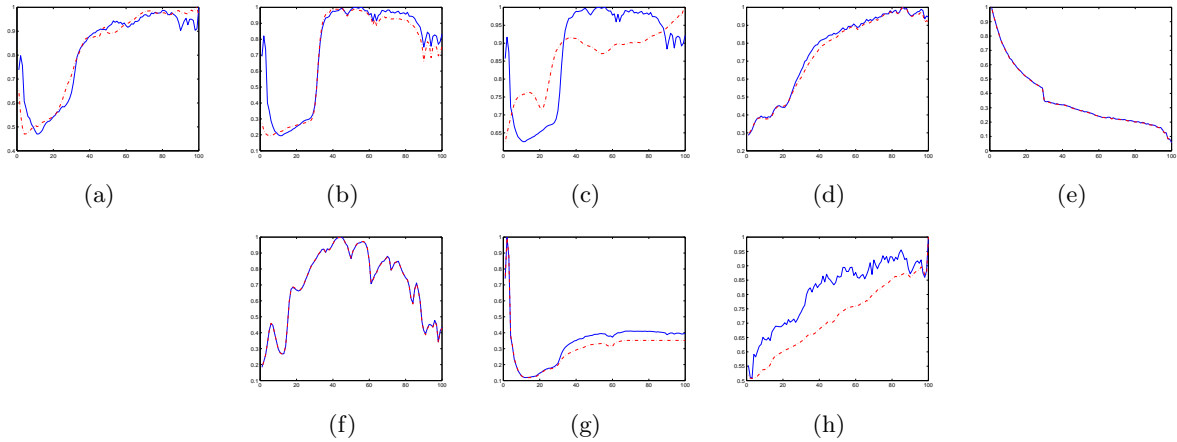


Figure 7. (The blurred and noisy tensor image) The original material spectral signatures: red and - . and the estimated spectral signatures: blue and - : (a) Bolts; (b) Copper Stripping,; (c) Hubble Honeycomb Side; (d) Hubble Honeycomb Top; (e) Hubble Aluminum; (f) Hubble Green Glue; (g) Solar Cell and (h) Black Rubber Edge.

Table 1. Materials, colors and fractional abundances used for Hubble satellite simulation.

Material	Color	Fractional Abundance (%)
Bolts	red	3
Copper Stripping	cyan	13
Hubble Honeycomb Side	blue	3
Hubble Honeycomb Top	white	4
Hubble Aluminum	light gray	19
Hubble Green Glue	dark gray	12
Solar Cell	gold	37
Black Rubber Edge	dark gray	8

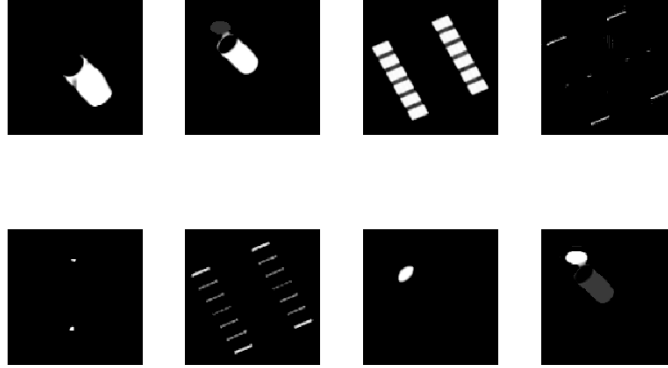


Figure 8. Segmented eight materials using the moving average method on the original HST tensor.

4.3 Moving Average Segmentation Results

We have applied the moving average method, or specifically the average normalized cross-correlation function in (11), to the aforementioned four HST datasets, namely the original, the noisy, the blurred, and the noisy and blurred, using the eight material spectral traces shown in Figure 1, i.e. $f_i(\lambda)$ in (11). The segmented material areas are respectively shown in Figures 8 to 11. An 8×8 pixel array is chosen as the averaging cell \mathcal{C} . The average normalized correlation function (10) is applied on an extremely noisy HST dataset with $SNR = 1$, shown in the left of Figure 12, in which the profile of HST can not be discerned, but the denoised figure on the right clearly shows the profile. Here the averaging cell size is 4×4 .

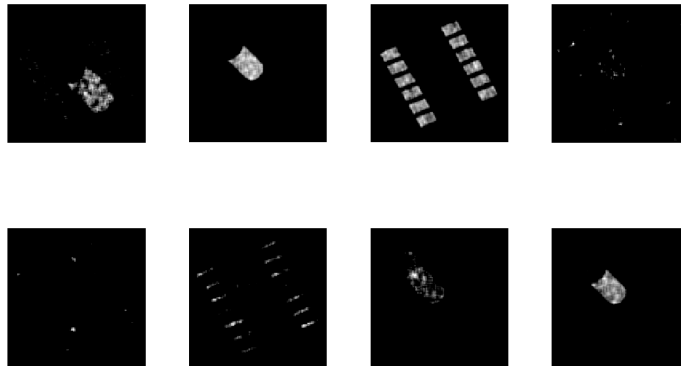


Figure 9. Segmented eight materials using the moving average method on the noisy HST tensor ($SNR=3$).

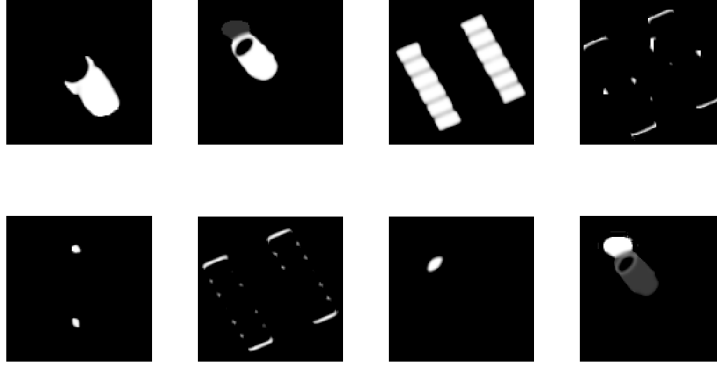


Figure 10. Segmented eight materials using the moving average method on the blurred HST tensor.

5. SUMMARY AND FURTHER WORK

We have proposed two approaches for segmenting hyperspectral images, a variational fuzzy clustering method and a statistical moving average method. A combined variational image restoration and segmentation model for hyperspectral space object unsupervised material identification in the presence of noise and blur is has been developed for images and extended to hyperspectral case. Numerically, the model is solved by a convergent alternating minimization method. Numerical results show that this proposed method is a promising approach to hyperspectral material identification associated with space object identification. Note that these spectral traces, sometimes called endmembers, are determined here without matching with a spectral library as is often used.

In addition, we have considered a particularly simple segmentation approach which makes use of the spatial variation of spectral correlation in a typical hyperspectral dataset. Apart from its simplicity, the approach is largely forgiving of any flux variations from pixel to pixel of a specific material. The approach is also robust against noise and blur. Any zero-mean noise that is uncorrelated from pixel to pixel and one spectral channel to the next is essentially averaged to zero because of the joint spectral and spatial averaging contained in the expressions (10) and (11). The robustness against blur may be traced to the fact that for each material the method uses information in multiple spatial pixels and spectral channels, thus greatly constraining the segmentation problem.

Both approaches are illustrated by the considering satellite material identification. Tests indicate that each method is promising. Further work and comparisons on additional data are needed to quantify the findings. Another, rather different, approach to obtaining compressive representation of hyperspectral data has been recently investigated by Gillis and Plemmons.¹⁸ There, the authors present a new variant of nonnegative matrix factorization called Nonnegative Matrix Underapproximation (NMU), based on the introduction of underapproximation constraints which enables one to extract features in a recursive way, like PCA, but preserving nonnegativity. These additional constraints make NMU well-suited to achieve a parts-based and sparse representation of the data, enabling it to recover the constitutive elements in hyperspectral data. A comparison will be made between the methods proposed here with the methods in¹⁸ on a variety of hyperspectral data cubes, including ARVIS and HYDICE data.

REFERENCES

- [1] Q. Zhang, H. Wang, R. Plemmons, and P. Pauca, “Tensor Methods for Hyperspectral Data Analysis: A Space Object Material Identification Study”, *Journal of the Optical Society of America, A.*, Vol. 25, No. 12, pp. 3001-3012, December, 2008.
- [2] D. Chen and R. Plemmons, “Nonnegativity constraints in numerical analysis”, in “The Birth of Numerical Analysis”, A. Bultheel and R. Cools, Eds., World Scientific Press, 2009.
- [3] T. Blake, S. Cain, M. Goda, and K. Jerkatis, “Enhancing the resolution of spectral images”, *Proc. SPIE* 6233, 623309 (2006).

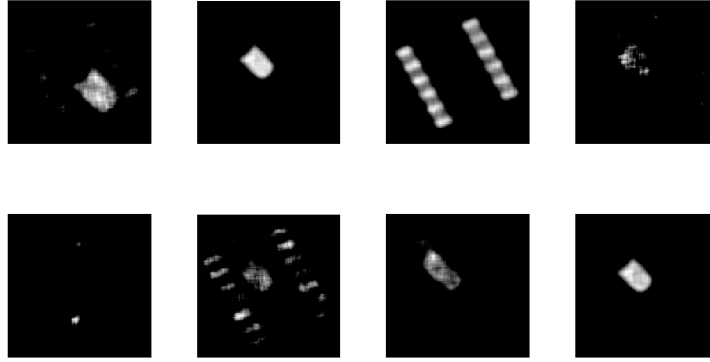


Figure 11. Segmented eight materials using the moving average method on the blurred and noisy HST tensor (SNR=3).

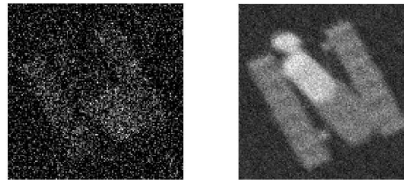


Figure 12. Denoising an extremely noisy HST tensor using the moving average method (SNR=1).

- [4] T. Blake, S. Cain, M. Goda, and K. Jerkatis, "Reconstruction of spectral images from the AEOS spectral imaging sensor", Proceedings of AMOS Technical Conference (Maui, 2006).
- [5] Y. Du, C-I. Chang, H. Ren, C-C. Chang, J.O. Jensen and F.M. D'Amico, "New hyperspectral discrimination measure for spectral characterization", *Optical Engineering*, 43, pp. 1777-1786 (2004).
- [6] K. Hege, D. O'Connell, W. Johnson, S. Basty and E. Dereniak, "Hyperspectral imaging for astronomy and space surveillance", *Imaging Spectrometry IX*, S. Chen and P. Lewis eds., Proc. SPIE 5159, 380-391 (2003).
- [7] Z. Guo, T. Wittman and S. Osher, " ℓ_1 Unmixing and its Application to Hyperspectral Image Enhancement", in *Algorithms and Technologies for Multispectral, Hyperspectral, and Ultraspectral Imagery XV*. Edited by S. Shen and P. Lewis, Proceedings of the SPIE, Volume 7334, pp. 73341M-73341M-9, 2009.
- [8] C. Van Loan, "Future directions in tensor-based computation and modeling", (2009). Available at <http://www.cs.cornell.edu/cv/TenWork/FinalReport.pdf>.
- [9] T. F. Chan and L. A. Vese, "Active contour without edges", *IEEE Trans. Image Proc.*, 10 (2001), 266-277.
- [10] L. Pi, C. Shen, F. Li, and J. Fan, "A variational formulation of segmenting desired objects in color images", *Image and Vision Computing*, vol. 25, pp. 1414-1421, 2007.
- [11] M.C. Roggemann and B. Welsh, *Imaging Through Turbulence*, CRC Press, (1996).
- [12] Y. Huang, M. Ng and Y. Wen, "A fast total variation minimization method for image restoration", *SIAM Journal on Multiscale Modeling and Simulation*, vol. 7, pp. 774-795, 2008.
- [13] A. Chambolle, "An algorithm for total variation minimization and applications", *J. Math. Imaging Vis.*, vol. 20, no. 1-2, pp. 89-97, 2004.
- [14] H. Liao, F. Li, and M. K. Ng, "Generalized cross-validation for total variation image restoration", *Journal of the Optical Society of America, A.*, 26 (2009), pp. 2311-2320.
- [15] D. Mumford and J. Shah, "Optimal approximations by piecewise smooth functions and associated variational problems", *Comm. on Pure and Applied Mathematics*, 42(1989), pp. 577-685.
- [16] S. Prasad, Q. Zhang, and R. Plemmons, in preparation.
- [17] F. Li, M. Ng, and R. Plemmons, "Coupled Segmentation and Denoising/Deblurring Models for Hyperspectral Material Identification", Preprint, November 2009.
- [18] N. Gillis and R. Plemmons, "Dimensionality reduction, classification, and spectral mixture analysis using nonnegative underapproximation", Preprint, December 2009.